Chemically Selective Soft X-ray Direct-Write Patterning of Multilayer Polymer Films

Jian Wang, Harald D. H. Stöver, and Adam P. Hitchcock*

Department of Chemistry and Brockhouse Institute for Materials Research, McMaster University, Hamilton, Ontario, Canada L8S 4M1

Received: April 2, 2007; In Final Form: July 4, 2007

Chemically selective soft X-ray direct-write patterning of trilayer polymer films was performed in a scanning transmission X-ray microscope, extending recent pioneering work on bilayer polymer films. Two trilayer polymer systems were examined: PMMA/PPC/PAN and PMMA/PEC/PAN, where PMMA = poly(methyl methacrylate), PPC = poly(propylene carbonate), PAN = polyacrylonitrile, and PEC = poly(ethylene carbonate). Each polymer layer was selectively patterned by exposure at its characteristic absorption energy: 288.45 eV for PMMA, 290.40 eV for PPC (PEC), and 286.80 eV for PAN. The patterns were visualized by imaging at these same energies. For the PMMA/PPC/PAN trilayer, highly selective patterning was achieved for the PAN and PPC layers, while the selectivity for the PMMA layer was poor. This was significantly improved by replacing PPC with PEC. The trilayer patterning process was simulated from the X-ray absorption spectra of the polymers, the layer order and thicknesses, and the critical doses for damage of each polymer. The simulations give semiquantitative predictions of the experimental contrast, and are a useful tool to find exposure times that optimize pattern contrast. Methods to improve patterning selectivity are discussed. Full color pattern reproduction with ∼150 nm spatial resolution is demonstrated with several high-resolution patterns created in the PMMA/PEC/PAN trilayer film.

1. Introduction

Selective control of chemical reactions has always been a fundamental goal of chemistry. In order to achieve it, photochemistry is especially efficient since the resonant character of photoabsorption can be used to selectively initiate a reaction in a specific target species. The cross sections for soft X-ray (100−1000 eV) absorption are large and lead to significant chemical modification. Since the near-edge X-ray absorption fine structure (NEXAFS) spectra[1] of many species have intense resonances at unique energies, these have great potential as a basis for chemically selective photochemistry. However, secondary processes associated with photoabsorption, such as radical/ion generation and spreading, have deteriorated this selectivity by transferring energy and damage from the initial absorption species to adjacent species which do not absorb the primary radiation. Recently we surmounted this problem and demonstrated chemically selective direct-write patterning using monochromated soft X-rays[2] in a scanning transmission X-ray microscope (STXM).[3,4] The key is to use a layered polymer system, where the interface, through a mechanism as yet incompletely understood, acts as a barrier to transfer of the radiation damage between layers. As a result, we successfully demonstrated a basic bilayer strategy that allows complex patterns to be selectively transferred to target layers with submicron spatial resolution and high chemical contrast, i.e., patterning one layer without damaging the other layer.[2] Without the layer structure, i.e., if the different chemical species were intimately mixed as in a blend, all components are damaged with exposure at any energy, as shown previously.[2]

Here we present the extension of this approach to a trilayer film which allows “full color” pattern reproduction on the submicron scale (∼150 nm line widths). This trilayer consists of three different chemical species that have intense absorption bands at energies where the other two species have weak absorption (orthogonal absorption bands). Specifically, the previously used polyacrylonitrile (PAN) and poly(methyl methacrylate) (PMMA) bilayer components were augmented with a third polymer which has strong absorption at its own unique energy and limited absorption at the PAN and PMMA characteristic energies. The polymers found to be suitable are aliphatic polycarbonates, such as poly(propylene carbonate) (PPC) and poly(ethylene carbonate) (PEC). The chemical structures of PPC, PEC, PMMA, and PAN are given in Scheme 1. In order to guide the optimization of trilayer systems capable of “full color” reproduction, a program to simulate radiation damage in multilayer polymer systems has been developed. It combines key input data (the quantitative NEXAFS spectra, layer thicknesses, layer order, and exposure protocol) to reproduce the experimental observations, and to predict optimum exposure protocols, thereby enabling rational optimization of multilayer systems for chemical patterning using tunable, monochromatic X-rays.

This paper is organized as follows. Section 2 describes experimental methods. Section 3 describes the principles to simulate chemically selective patterning in multilayer polymer films. Section 4 presents the NEXAFS spectra and damage kinetics for PAN, PMMA, PPC, and PEC, and the results from chemically selective patterning of the PMMA/PPC/PAN and PMMA/PEC/PAN trilayers. The two systems are compared with regard to patterning selectivity. Several demonstrations of chemically selective patterning in the PMMA/PEC/PAN trilayer are then presented. We conclude by suggesting methods to further optimize chemical patterning with multiple wavelength monochromated X-rays and possible extensions to other applications.

* Corresponding author. Telephone: (905) 525-9140, ext 24749. Fax: (905) 521-2773. E-mail: aph@mcmaster.ca.

10.1021/jp072570s CCC: $37.00 © 2007 American Chemical Society
Published on Web 10/04/2007

SCHEME 1: Chemical Structures of Poly(methyl methacrylate) (PMMA), Polyacrylonitrile (PAN), Poly(propylene carbonate) (PPC), and Poly(ethylene carbonate) (PEC)

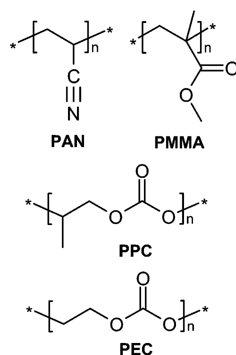

2. Experimental Section

2.1. Sample Preparation. PAN (M_w = 150K) was obtained from Aldrich; PMMA (M_w = 312K) was obtained from Polymer Source Inc.; PPC (M_w = 250K) and PEC (M_w = 150K) were obtained from Empower Materials. All polymers were used without further purification. For NEXAFS spectroscopy and critical dose measurements, free-standing single layer films of each polymer were made according to the same procedure of ref 2. First, a 1 wt % solution of each polymer was prepared in suitable solvents, which were *N*,*N*-dimethylformamide (DMF) for PAN, toluene for PMMA, and 1,4-dioxane for both PPC and PEC. Then a ~50 μL drop of each solution was spun cast (3000 rpm, 30 s) onto freshly peeled, 2.5 cm × 2.5 cm mica surfaces. The room-temperature spun cast PMMA film was used as formed. The PAN, PPC, and PEC single layer films were dried under vacuum at 70 °C for 0.5 h to remove all solvents. Subsequently, all films were cut into 3 mm × 3 mm pieces on the mica surfaces, and then floated onto Milli-Q water. A piece of the polymer film was transferred to a degreased hexacomb grid or a TEM grid and used for STXM measurements after drying again in ambient. The single layer films formed under the above conditions were 30−40 nm thick, according to STXM measurements.

Free-standing trilayer films of PAN (bottom), PPC or PEC (middle), and PMMA (top) were fabricated by spin coating successively, first, PAN from DMF, second, PPC or PEC from 1,4-dioxane, and, third, PMMA from toluene onto the same mica substrate as described above. After each spin coating, the drying condition of each deposited layer was the same as that of the single layer preparation outlined above. The solvents and order of the layers were carefully selected so that the solutions applied on top of an already deposited layer would not dissolve the previously fabricated polymer film. Relative solubility data are summarized in Table 1. Reversing the spin coating sequence for any two of the three polymers will result in a nonuniform microphase-separated film due to redissolution of the already deposited layer, as shown in ref 2. It is rather difficult to find fully orthogonal solvents for these non-cross-linked polymers. Thus, only some layer sequences are viable using the successive spin coating procedure, which we prefer as it gives the most uniform thickness of the layers. The average thickness of the resulting trilayer film was 105(10) nm according to STXM measurements, in close agreement with the value of 120(15) nm determined from the height profile across a scratch through the trilayer film measured by atomic force microscopy (AFM; Quesant Q-scope 350).

2.2. STXM. Experiments were performed at the Advanced Light Source beamline 5.3.2[5] using the polymer scanning transmission X-ray microscope (STXM).[6] The settings of the microscope and the beamline, as well as the procedure for radiation damage studies, were presented elsewhere.[2,7] In brief, a single layer film of each polymer was exposed at 300 eV with an incident photon flux of 1.5−2.5 MHz in the focused ~50 nm diameter X-ray spot. The detector efficiency is 30 ± 10% in the C 1s region,[6,7] and thus the actual incident photon flux is about 3 times larger. A N_2 gas filter (0.7 Torr for a 1 m path) was used to ensure there was negligible higher order radiation, which would result in errors in the quantitative dose−damage evaluation. After a series of exposures at different regions on the polymer film, analysis images were recorded at the characteristic absorption energies for each polymer. In these images, the best contrast between damaged and undamaged regions is displayed. The characteristic absorption energies for the polymers in this work are the strong C 1s → π* transitions: 286.80(5) eV for PAN, 288.45(5) eV for PMMA, and 290.40(5) eV for PPC and PEC. The damage rate was evaluated from the dose−damage profile, which plots the damage, expressed as the change in optical density (absorbance) at the characteristic energy, as a function of radiation dose (in units of gray, where 1 Gy = 1 J/kg), determined from the exposure time, incident flux, and absorbance, as outlined elsewhere.[2,7] The dose−damage curve was analyzed assuming first-order kinetics,[2,7−11] i.e., an exponential rise of the damage signal to a maximum value at infinite dose (see eq 3 of ref 2). The fit determines the critical dose of the polymer, i.e., the radiation dose required to attenuate a specific spectroscopic feature to 1/e of the initial intensity. The higher the critical dose, the slower the damage rate.

The chemically selective patterning experiments were performed using the same pattern generation program and procedure as in ref 2. Specifically, the sample is positioned with ~10 nm precision under laser interferometer control[6] to predefined (x,y) locations and then a fast-acting (~300 μs) in-vacuum piezo shutter is opened for a precise, predefined, position-dependent time interval (usually 50−500 ms) to expose the sample to the focused monochromated soft X-rays. The input files for pattern generation are lists of (x, y, t, E) values for each pixel, which are prepared from color-separated images by a routine in aXis 2000.[12] The overall physical size, the pixel density, and thus sampling resolution of the input pattern can be adjusted by changing the image characteristics prior to generating the pattern generation input file. For multicolor (multiphoton energy) patterns, the input files for each color are written sequentially at the appropriate photon energies.

TABLE 1: Solubility of Selected Polymers in Selected Solvents[a]

polymer	solvent DMF	1,4-dioxane	toluene
PAN	+	−	−
PPC	+	+	−
PEC	+	+	−
PMMA	+	+	+

[a] +, soluble; −, insoluble.

3. Simulation of Chemically Selective Patterning in Multilayer Polymer Systems

If quantitative NEXAFS spectra and critical doses for each polymer of a multilayer system are known, it is possible to simulate the chemically selective patterning (or damage) that will result from a defined exposure protocol. For this, it is assumed that (i) first-order damage kinetics apply,[2,7−11] (ii) there

is negligible mass loss in the dose range comparable to the critical dose, and (iii) damage is not transferred between adjacent layers.[2] The total optical density (OD) of a multilayer system at any energy, E, is given by

$$\mathrm{OD}(E) = \sum_i l_i A_i(E) \tag{1}$$

where l_i is the thickness of the ith layer and $A_i(E)$ is the linear absorption coefficient (i.e., OD per nanometer) of component i at photon energy, E. The thickness of each layer is determined by fitting the measured total C 1s spectrum to the linear absorption coefficients of all the components.

For the chemically selective patterning of a target layer, the exposure energy is chosen at its characteristic absorption energy for best patterning selectivity, even though damage to other layers also occurs due to their small photoabsorption at this energy. Thus the simulation is performed by separately computing the radiation damage in each layer with a defined exposure protocol. Specifically, for given energy and exposure time, the remaining OD at the damaged region of a selected layer is calculated according to eq 2, which incorporates both damage kinetics and dose evaluation:[2,7,11]

$$\mathrm{OD}_t = \mathrm{OD}_\infty + C \exp\left[-\frac{I_0(1 - \mathrm{e}^{-\mathrm{OD}})Et}{\epsilon V \rho a_\mathrm{c}}\right] \tag{2}$$

where OD_t is the remaining optical density of the exposed region, OD_∞ is the extrapolated optical density after infinite dose, C is a constant, which is equal to the infinite damage ($D_\infty = \mathrm{OD}_0 - \mathrm{OD}_\infty$, where OD_0 is the initial optical density) in the case of negligible mass loss, I_0 is the incident flux (note the incident flux for each successive layer is the flux transmitted through the previous layer), OD is the dynamic optical density of the exposed region during irradiation, which is assigned to OD_0 for simplicity, E is the photon energy, t is the exposure time, ϵ is the detector efficiency, V is the volume of the exposed region (considered to be the volume of a single pixel = 60 nm × 60 nm × l_i), ρ is the polymer density, and a_c is the critical dose of the selected polymer.

The pattern quality is related to the change in OD in the damaged region relative to the undamaged region. There are several ways to define image contrast. The definition of image *contrast* used in this work is

$$\mathrm{contrast} = \frac{\mathrm{OD}_0}{\mathrm{OD}_t} \tag{3}$$

More radiation damage in a given layer means a higher value of the contrast in that layer. Contrast values are always greater than 1, and are independent of layer thickness, within the formalism above. Patterning *selectivity* is then related to the relative contrast in each layer, and can be defined for the purpose of optimization in a pairwise fashion for layers a and b as

$$\mathrm{selectivity(a{:}b)} = S_\mathrm{ab} = \frac{\mathrm{contrast(a)}}{\mathrm{contrast(b)}} \tag{4}$$

The contrast is not a linear function of exposure time; thus patterning selectivity varies with exposure time, as well as other aspects of the multilayer system, such as layer order and thickness. The best selectivity would correspond to the greatest differentiation among the pattern contrast in different layers, which can be predicted by consideration of an*optimizer* that simultaneously maximizes all pairwise selectivities. In a trilayer system such an optimizer can be defined as

$$\mathrm{optimizer} = S_\mathrm{ab} + S_\mathrm{ac} + S_\mathrm{bc} \tag{5}$$

The best exposure protocol for chemically selective patterning is that which maximizes the value of this optimizer. ChemLith is an Excel application program developed to simulate chemically selective patterning for multilayer polymer systems within the framework outlined above. Factors that may influence the selectivity, such as layer order, layer thickness, materials (and thus NEXAFS spectra and critical dose), choice of exposure energy, time, and incident flux, can all be analyzed and optimized.

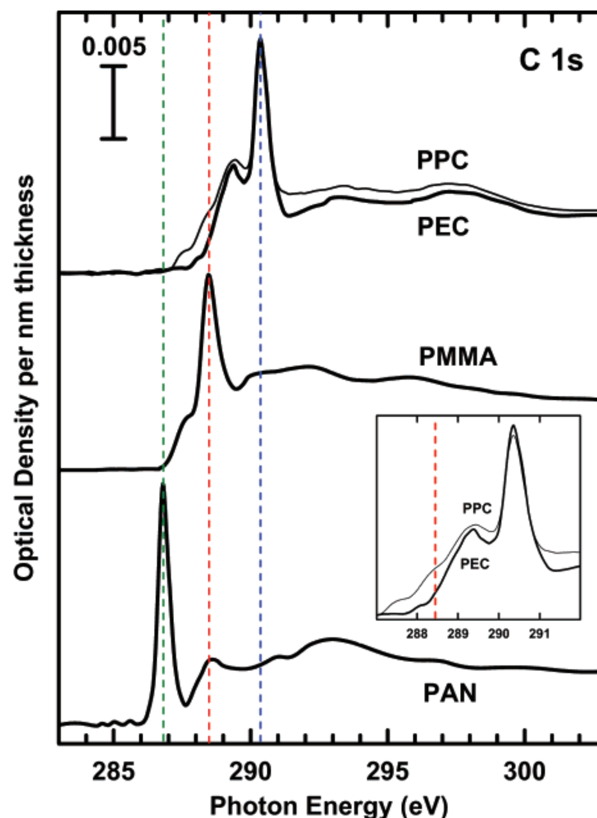

Figure 1. C 1s NEXAFS spectra of PMMA, PAN, PPC (thinner line), and PEC (thicker line). The vertical dashed lines indicate the energies used to create patterns in each species. The inset expands the spectra of PPC and PEC in the energy region used for PMMA patterning.

4. Results

4.1. NEXAFS Spectra and Critical Doses for PMMA, PAN, PPC, and PEC. Figure 1 presents the spectra of undamaged PPC, PEC, PAN, and PMMA. Radiation damage of PAN and PMMA causes spectral changes which are readily observed in the C 1s NEXAFS spectra.[2,7] The main change is a decrease of the strong C 1s → π^* transitions. Other spectral changes also occur, including the appearance and growth of a new feature at 285 eV and a decrease in the C 1s continuum intensity. The former signal is associated with C 1s → $\pi^*_{\mathrm{C=C}}$ transitions arising from C═C bonds formed in the damaged polymer backbone. The decreased continuum intensity is associated with mass loss. Since the change of the C 1s → π^* transition intensity is the most sensitive to damage, this signal has been used to evaluate damage and patterning contrast in this study. The quantitative NEXAFS spectra of PPC and PEC are very similar except that the spectrum of PEC has less

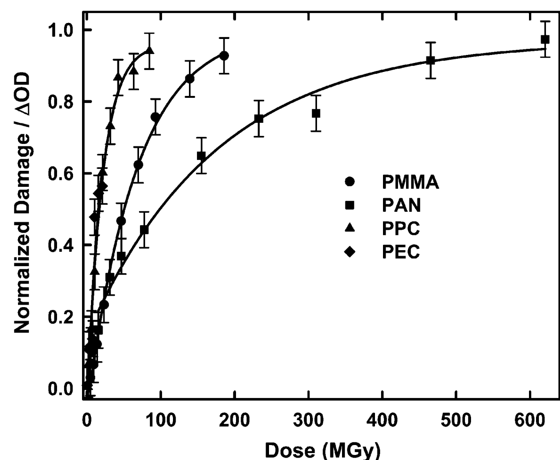

Figure 2. Damage versus dose curves for PMMA, PAN, PPC, and PEC derived from STXM measurements at the C 1s edge. The exposure energy was 300 eV. The damage signal, which is the normalized change in optical density monitored at the characteristic photon energies, tracks the amount of damaged product and thus integrates over possible differences in damage rates for different mechanisms.

absorbance between 287 and 289 eV due to the absence of a methyl group (see insert to Figure 1). Radiation damage to PPC and PEC is also characterized by a substantial decrease of the C 1s → $\pi^*_{C=O}$ transition at 290.40 eV. In addition there is considerable mass loss, as evidenced by a decrease in the C 1s continuum intensity with increasing dose.

Figure 2 plots the damage (change of OD at the C 1s → π^* transition) normalized to infinite damage (D_∞) versus radiation dose for PAN, PMMA, PPC, and PEC, derived from STXM measurements for the pure polymers. All the samples were irradiated at 300 eV in the C 1s continuum for less absorbance variation during radiation damage. The critical dose for soft X-ray damage should be an inherent property of a polymer, and thus the critical dose at the π^* resonance is expected to be the same as that at 300 eV. Note that the dose rate at different energies will vary because of the different absorbance values but this is taken into account in computing dose. The quantitative damage was evaluated from changes in optical density at the characteristic absorption energies (C 1s → π^* transitions). The damage signal for each species was normalized to the infinite damage level for that species, in order to compare the relative amount of damage created for the same dose. Qualitatively, the relative damage rates are PPC ≈ PEC > PMMA > PAN. Quantitative evaluation of the data in Figure 2 by a fit to eq 3 of ref 2 (or a modification of eq 2 in this work) gave critical doses of 150(20) MGy for PAN, 60(10) MGy for PMMA, and 25(5) MGy for PPC and PEC. The critical dose for PMMA determined in this work is consistent with literature values obtained at different irradiation photon energies.[8,11]

4.2. Chemically Selective Patterning for PMMA/PPC/PAN Trilayer. The selective patterning for a bilayer system, PMMA/PAN, has been demonstrated previously[2] with high selectivity and good image contrast. Our goal in this work was to add a third layer to the PMMA/PAN bilayer system, in order to enable full color, chemically sensitive patterning. The choice of the third layer can be rather challenging. The polymer of the third layer should have (i) a chemically distinct absorption feature with a large OD, which is shifted by at least ~1 eV with respect to the other two layers for complete peak separation; (ii) a suitable damage rate in terms of critical dose; and (iii) relatively little absorption at the photon energies used to damage PMMA or PAN. This has led us to explore aliphatic instead of aromatic polymers, since the phenyl components of aromatic polymers are very damage resistant.[7,13,14] Three generic polymer systems were examined as the third layer: aliphatic polyurethane, aliphatic polyurea, and aliphatic polycarbonate. Aliphatic polycarbonates turned out to be the best, since they are commercially available, have high molecular weights, and are soluble in an appropriate solvent for spin coating.

The first trilayer system that was successfully fabricated and patterned was PMMA/PPC/PAN. The notation indicates the ordering of the three layers, with the first mentioned species being the upstream layer (upstream refers to the layer first hit by the incident X-rays). Figure 3a shows ChemLith predictions of the contrast in each layer as a function of exposure time, for the PMMA/PPC/PAN trilayer. The layer thicknesses for the trilayer patterned and analyzed by STXM are 27(3) nm of PMMA, 27(3) nm of PPC, and 36(4) nm of PAN. The top panel of Figure 3a plots the contrast as a function of exposure time created in each of the three layers by irradiation at 288.45 eV. The contrast is defined as in eq 3, and the incident fluxes (I_0) are 2.0, 1.8, and 2.3 MHz at 288.45, 290.40, and 286.80 eV, respectively. Figure 3a shows that while PMMA and PAN are well differentiated (PMMA damage is much higher than PAN damage at most exposure times), this is not the case for PMMA and PPC. In fact, the contrast as a function of exposure time in the PMMA layer is very similar to that created in the PPC layer, even though the PPC is being damaged by an energy different from the energy of its characteristic C 1s → $\pi^*_{C=O}$ peak. This predicts that the patterning selectivity of the PMMA layer would be very poor. The middle and bottom panels of Figure 3a present the contrast profiles for selective patterning of the PPC and PAN layers at 290.40 and 286.80 eV, respectively. In contrast to exposure at 288.45 eV, much better selectivity can be seen for these energies in that the contrast generated in PPC by exposure at 290.40 eV is much higher than that in PMMA or PAN, and the contrast generated in PAN by exposure at 286.80 eV is much higher than that in PMMA or PPC.

To verify the quantitative accuracy of the simulations, a series of exposures at variable exposure time were carried out for the same PMMA/PPC/PAN trilayer using the input pattern displayed in Figure 4a. It is a three-color version of the logo of Lawrence Berkeley National Laboratory (LBNL), which is composed of a roof pattern in red, a window pattern in blue, and a tower pattern in green. The red pattern was written into the PMMA layer by exposing at 288.45 eV to selectively damage the ester group; the blue pattern was written into the PPC layer by exposing at 290.40 eV to selectively damage the carbonate group; the green pattern was written into the PAN layer by exposing at 286.80 eV to selectively damage the cyanide group. The incident flux was measured to be 2.0, 1.8, and 2.3 MHz at 288.45, 290.40, and 286.80 eV, respectively. Then LBNL logo patterns were patterned with chemical selectivity into the PMMA/PPC/PAN trilayer with combinations of exposure time selected from 50, 100, and 250 ms at 288.45 eV for the roof pattern; 50, 100, and 200 ms at 290.40 eV for the window pattern; and 100, 200, and 500 ms at 286.80 eV for the tower pattern. For each created logo pattern, the contrast in each layer was extracted from the experimental optical density image at the corresponding characteristic energy based on eq 3. The experimentally determined contrast for each pattern is also plotted in Figure 3a in comparison with the contrast predicted by ChemLith. The results show that the contrasts in the observed patterns are close to the contrast predicted by the simulations at relatively short exposure times, i.e., lower doses. For longer exposure times, some experimental results deviate from the simulations, probably due to errors in the dose−damage model,

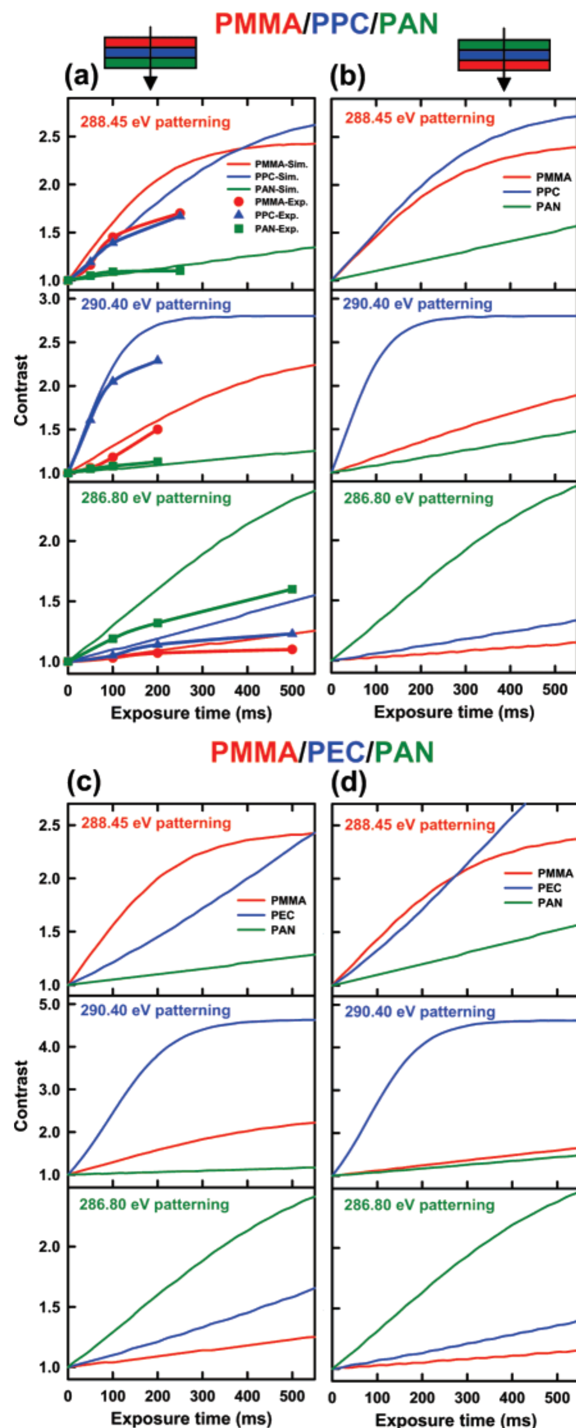

Figure 3. Simulations and experimental results for chemically selective patterning of PMMA/PPC/PAN and PMMA/PEC/PAN trilayers. (a) Predicted contrast (thinner lines) as a function of exposure time for a PMMA/PPC/PAN trilayer with a layer thickness profile as 27/27/36 nm. The top panel shows the contrast as a function of exposure in each of the three layers for exposure at 288.45 eV with $I_0 = 2$ MHz; the middle panel shows the contrast in each of the three layers for exposure at 290.40 eV with $I_0 = 1.78$ MHz; the bottom panel shows the contrast in each of the three layers for exposure at 286.80 eV with $I_0 = 2.25$ MHz. The points and thicker lines plot the experimentally observed contrast as a function of exposure time for selective patterning of each layer under the same incident fluxes. (b) Predicted contrast for the same trilayer system as in (a) but with the PAN layer upstream and thus first exposed to the X-ray beam. (c) Predicted contrast as a function of exposure time for a PMMA/PEC/PAN trilayer with layer thicknesses of 41/46/33 nm under the same exposure energies and I_0 values as (a). (d) Predicted contrast as a function of exposure time for the same trilayer system as (c), but with the PAN layer upstream.

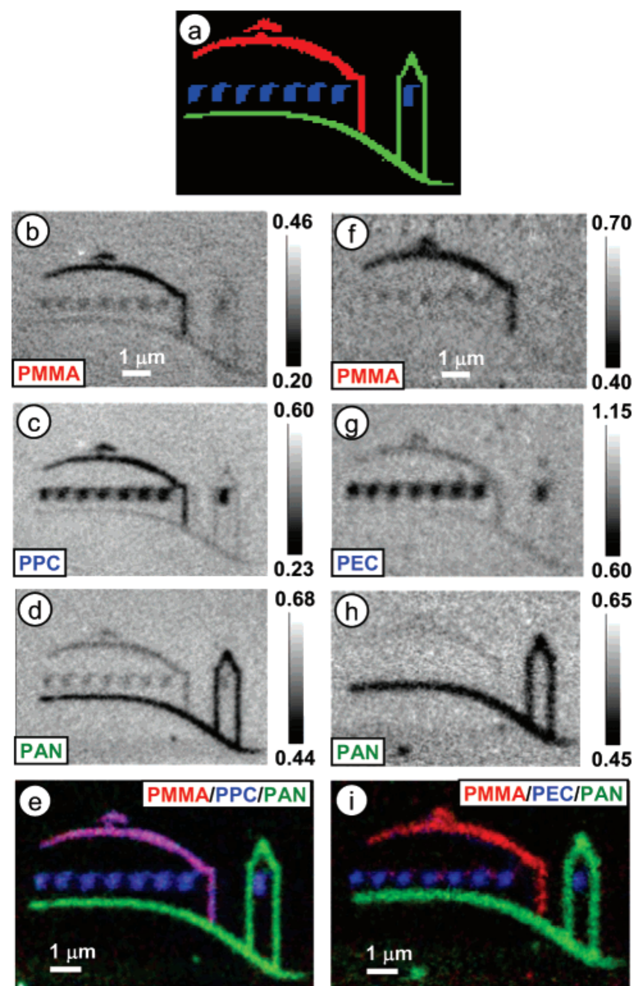

Figure 4. Demonstration of chemically selective patterning of the LBNL logo into PMMA/PPC/PAN and PMMA/PEC/PAN trilayers. (a) Input file, with the roof (red) patterned at 288.45 eV (PMMA), the windows (blue) patterned at 290.40 eV (PPC and PEC), and the tower (green) patterned at 286.80 eV (PAN). (b) Optical density image of the patterned region viewed at 288.45 eV for the PMMA/PPC/PAN trilayer (PMMA absorbs strongest). (c) Optical density image of the pattern region viewed at 290.40 eV for the PMMA/PPC/PAN trilayer (PPC absorbs strongest). (d) Optical density image of the patterned region viewed at 286.80 eV for the PMMA/PPC/PAN trilayer (PAN absorbs strongest). (e) Color-coded composite of the three images after inversion (red, PMMA damage; blue, PPC damage; green, PAN damage). (f) Optical density image of the patterned region viewed at 288.45 eV for the PMMA/PEC/PAN trilayer. (g) Optical density image of the pattern region viewed at 290.40 eV for the PMMA/PEC/PAN trilayer. (h) Optical density image of the patterned region viewed at 286.80 eV for the PMMA/PEC/PAN trilayer. (i) Color-coded composite of the three images after inversion (red, PMMA damage; blue, PEC damage, green; PAN damage). Note the fidelity of creating images in each layer independent of the other two is well demonstrated, but the images are blurred since the microscope was slightly out of focus during the pattern generation step.

such as mass loss and nonlinear behavior. This is especially true for selective patterning at 286.80 eV (PAN damage energy), for which the simulations significantly overestimate the contrast. Further studies are required to clarify the reason for this poor agreement. As predicted by ChemLith, the experimental results show that there is little selectivity between PMMA and PPC for the pattern written at 288.45 eV. The best selectivity for PPC was obtained at 100 ms, which is consistent with the predictions. Also, similar to the predictions, the longer the exposure time for PAN, the better the selectivity will be, but

the improvement was small. In conclusion, the simulations give useful qualitative guidance, but are only semiquantitative with regard to matching experiment.

Parts b, c, and d of Figure 4 present optical density images of the patterns created in the corresponding polymer layers of the PMMA/PPC/PAN trilayer with optimal exposure protocols of 100, 100, and 200 ms at 288.45, 290.40, and 286.80 eV, respectively. Both the radiation damage and the imaging were performed at the same energy. The tower and window patterns were selectively transferred to the PAN and PPC layers, respectively. However, the roof pattern was transferred with only marginal selectivity to the PMMA layer since that same pattern was also created in the PPC layer (Figure 4c). Figure 4e shows a color composite of the three patterned layers, where the individual images have been inverted to produce a black background. The colors of the tower and the windows are green and blue, respectively, indicating good chemical selectivity of patterning at the characteristic energies of the PAN and PPC components. However, the roof is purple, i.e., a nearly equal mixture of red and blue, corresponding to similar damage generated in both the PMMA and PPC layers when the roof pattern was generated at 288.45 eV.

Parameters that influence the patterning results have been explored using ChemLith in order to find ways to improve the patterning selectivity for the PMMA layer. Specifically, layer order and layer thickness have been investigated. Figure 3b presents the predictions of turning the film over so that the X-rays reach the PAN layer first before passing through the PPC and the PMMA layers. ChemLith predicts that the patterning selectivity for writing at 288.45 eV is even worse in this situation, with the PPC layer being damaged even more than the PMMA layer. However, the patterning selectivity for the PPC and PAN layers is further improved compared to the original order of the trilayer. We also explored another PMMA/PPC/PAN trilayer, one with different layer thicknesses due to a different sample preparation (23 nm PMMA, 48 nm PPC, 33 nm PAN). ChemLith predicted that patterning selectivity for all three layers is very similar to that for the system shown in Figure 3a with no improvement in selective patterning of the PMMA layer. This was confirmed by experiment (results not shown). This is not surprising since both the absorbed energy and the mass of material vary linearly with layer thickness, and thus to first order the dose (energy/mass) and thus the pattern contrast (as defined in this work) are independent of layer thickness. The only consequence of varying the thickness of a particular layer is to change the incident flux for the downstream layer(s) so that the relative contrast of the downstream layer(s) might be varied. By this logic, an increase of the PPC layer thickness cannot improve selective patterning of an upstream PMMA layer, especially with respect to the PPC layer. Finally, ChemLith does suggest that the selective patterning of the PMMA layer can be improved by increasing the layer thickness of just the PMMA layer. However, the improvement is very limited even if the layer thickness is doubled. Actually, the absolute linear absorbance of PMMA at 288.45 eV is ~3 times that of PPC (see Figure 1). At the same time, the critical dose of PPC is about 1/3 that of PMMA. Thus these two factors cancel each other, which has the net effect that the damage rate of PMMA and PPC are similar at 288.45 eV. That is why the selective patterning of PMMA is very poor. According to ChemLith, the best strategy to resolve this problem is to find another polymer that preserves the overall characteristics of PPC but has lower absorbance at 288.45 eV or has a larger critical dose.

4.3. Chemically Selective Patterning of a PMMA/PEC/PAN Trilayer. Poly(ethylene carbonate) (PEC), another polycarbonate polymer, was evaluated as a possible replacement for PPC. PEC retains most polymer and radiation damage properties of PPC but has a lower absorbance than PPC at 288.45 eV (see Figure 1) due to fewer C−H and C−C bonds per repeat unit. Figure 3c shows ChemLith simulations for a PMMA/PEC/PAN trilayer film, consisting of 41 nm PMMA, 46 nm PEC, and 33 nm PAN. The top panel of Figure 3c plots the contrast in each component as a function of exposure time for irradiation at 288.45 eV. Comparison to Figure 3a shows that the selective patterning of the PMMA layer should be significantly improved since the PMMA contrast is much higher than the PEC contrast, for the same exposure. The middle and bottom panels of Figure 3c represent the contrast as a function of exposure time for selective patterning of the PEC layer at 290.40 eV and the PAN layer at 286.80 eV. Once again, better patterning selectivity for the PEC layer and comparable selectivity for the PAN layer are predicted, compared to the PMMA/PPC/PAN trilayer. Figure 3d presents the predicted contrast (exposure) curves for the same PMMA/PEC/PAN trilayer system turned over to expose the PAN layer first. As found from examination of Figure 3b, the patterning selectivity becomes much worse for patterning at 288.45 eV, with very little difference in the contrast in the PMMA versus the PEC layer. Thus PMMA upstream is the preferred layer ordering even though the opposite layer ordering gives increased selectivity for the PEC and PAN layers.

To verify the above predictions, chemically selective patterning in the PMMA/PEC/PAN trilayer has been carried out, again using the LBNL logo as a test pattern. The exposure conditions (I_0 and dwell) for each polymer layer were the same as those used to pattern the PMMA/PPC/PAN trilayer. Parts f, g, and h of Figure 4 present optical density images of patterns created in PMMA, PEC, and PAN layers by exposure at 288.45, 290.40, and 286.80 eV, respectively. As shown in these images, all patterns were very selectively transferred to each corresponding polymer layer. The microscope was a little out of focus when the pattern generation was carried out, and thus the component maps and color composite (Figure 4i) are less sharp than the pattern in Figure 4e. In the composite map the colors are essentially pure red, pure blue, and pure green for each part of the logo pattern, indicating very good patterning selectivity.

Two other patterns were selectively written in the PMMA/PEC/PAN trilayer, with the results shown in Figure 5. The pattern in Figure 5a is composed of three circles with partial overlap to produce the seven major colors of the RGB color model. The right lower corner inset is the input image. The red, blue, and green patterns (circles) were selectively written into the PMMA, PEC, and PAN layers. The exposures were 125 ms/pixel for the PMMA and PEC layers and 250 ms/pixel for the PAN layer under the normal beamline conditions and the same microscope settings as before. Note that the exposure time needs to be adjusted when the incident flux deviates significantly from the previous values. Alternatively, entrance and exit slit sizes can be adjusted to give a similar incident flux. The generated color composite image (Figure 5a) clearly shows three circles with all seven colors well resolved, indicating high selectivity of the patterning. The point spacing used to write the pattern was a little too sparse, and thus the individual colors are slightly mottled relative to an optimum write. The pattern in Figure 5b shows a three-color version of the logo of McMaster University. The input pattern is shown. The same exposure conditions as those of the pattern in Figure 5a have been used, but a different color coding was used, i.e., PMMA

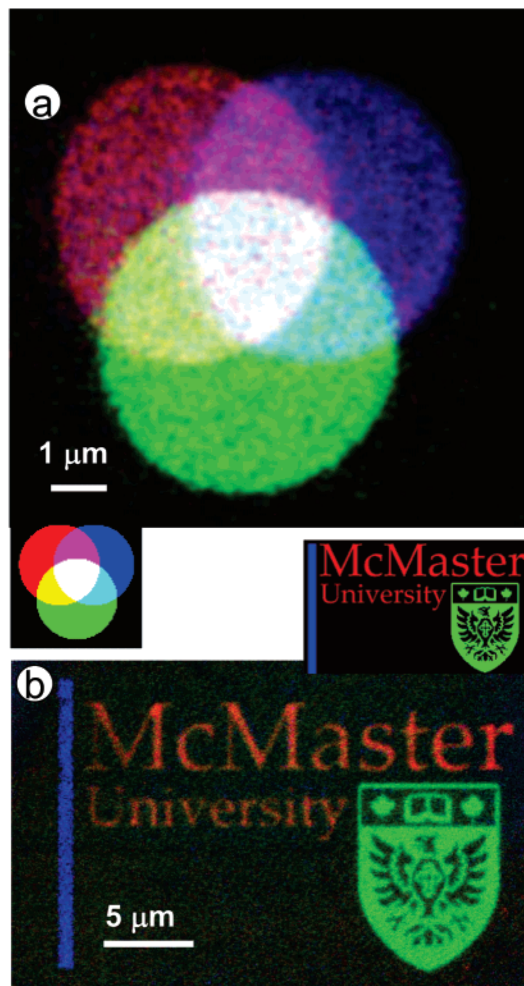

Figure 5. Chemically selective patterning of a PMMA/PEC/PAN trilayer. (a) RGB color circles (red, PMMA damage; blue, PEC damage; green, PAN damage). (b) Logo for McMaster University (red, PEC damage; blue, PMMA damage; green, PAN damage). The input is shown as inserts.

damage in blue, PEC damage in red, and PAN damage in green. Not only the correct colors but also the details of the pattern are clearly reproduced in the final composite image.

In order to demonstrate the layer order effect experimentally, a very simple pattern has been used, i.e., drawing one line in each polymer layer. To ensure that the lines are visible, the exposure time was increased to 250 ms/pixel for the PMMA and PEC layers, and 500 ms/pixel for the PAN layer, under the same beamline conditions and microscope settings. Figure 6a presents images of lines generated in the PMMA, PEC, and PAN layers with exposures at 288.45, 290.40, and 286.80 eV, respectively, for the original order of the trilayer; i.e., PMMA was upstream and thus received X-rays first. Figure 6b shows the results of the same line exposure protocol after the trilayer was turned over in the sample mount so that the PAN layer was upstream. Comparison of Figure 6a and Figure 6b shows that, in the reversed structure, the patterning selectivity for the PMMA layer at 288.45 eV is much worse since a strongly damaged line also appeared in the PEC layer at the same physical position, but the patterning selectivity for the PEC layer at 290.40 eV is greatly improved, as only the PEC layer was highly damaged at this energy. These phenomena are reflected in the color composite images in terms of a more purple color for the PMMA line and a more blue color for the PEC line in the composite image of the reverse order in Figure 6b.

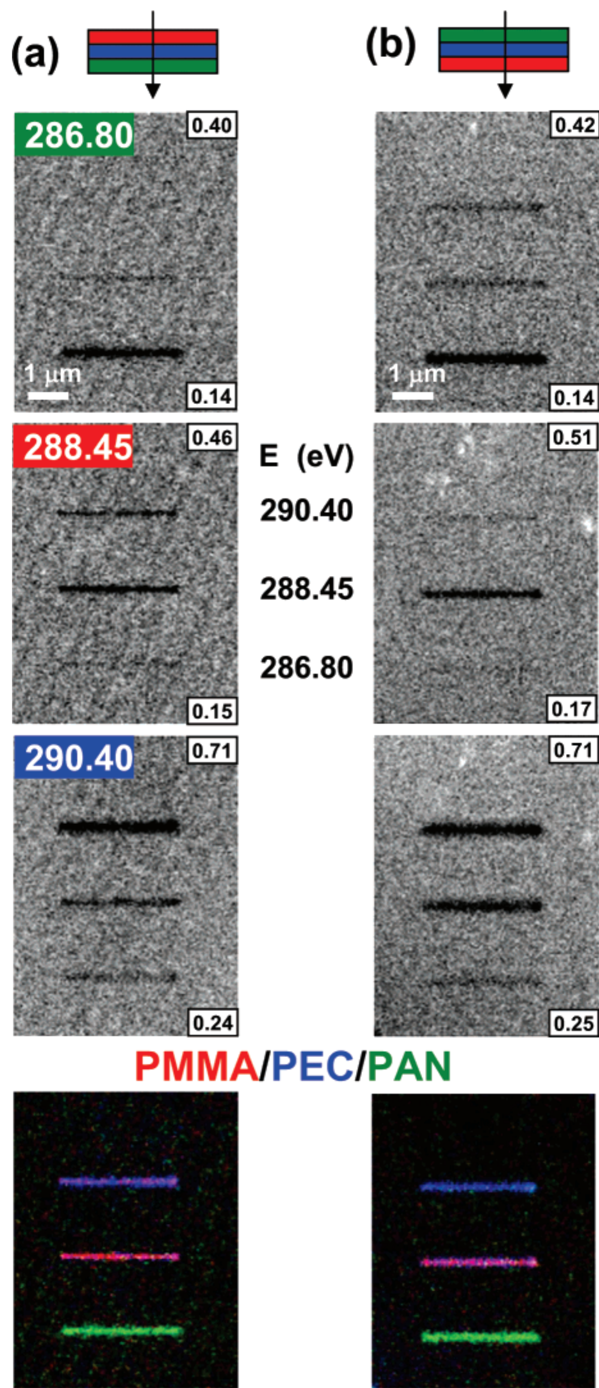

Figure 6. Comparison of chemically selective patterning of a PMMA/PEC/PAN trilayer and its reverse. (a) From top to bottom, optical density images of lines generated by exposure at 288.45, 290.40, and 286.80 eV, respectively, with the PMMA layer upstream; the color-coded composite image of the three patterned layers is shown at the bottom (red, PMMA damage; blue, PEC damage; green, PAN damage). (b) As for (a) but with the layer structure reversed so that the PAN layer is upstream.

Figure 6 shows that the width of the single-write lines with optimal focus and exposure is ~200 nm, as reported earlier.[2] This is surprising since many other applications of the STXM clearly show that the beam spot is less than 50 nm (for the zone plate used in this work the diffraction limited resolution is 42 nm)[15] and the position of the sample relative to the beam is interferometrically controlled to be stable at the 10 nm level.[6] Apparently, there is spreading of the radiation damage by some as yet not fully understood mechanism which broadens the lines.

Different aspects of radiation damage mechanisms were discussed in ref 2. In addition, Figure 6 shows that the damage line widths are different among these three polymers even though the extent of damage (relative to the critical dose for each species) was similar for each of them. The order of the line widths is PEC < PAN < PMMA. The difference is probably due to differences in damage mechanisms, damage propagation, and polymer chain reactions in these species. Further improvement in the spatial resolution of chemical patterning might be achieved by adding inhibitors to the polymer films to quench the radicals/ions produced by the X-rays.[16] Another approach could be to use very short exposures and then reveal the selective damage by chemical amplification.[17,18]

5. Discussion

Chemically selective patterning of trilayer polymer systems by tunable monochromated X-rays has been developed. This allows "full color" reproduction at the submicron scale. The simulation program (ChemLith) is able to provide semiquantitative predictions which were found to be useful in designing and optimizing multilayer systems for chemically selective patterning. Further improvements in chemical selectivity and spatial resolution would make this approach more powerful and thus potentially more useful. Both the NEXAFS spectroscopy and the critical dose for candidate polymers need to be considered simultaneously to improve patterning selectivity. Improvements in modeling the pattern contrast generation physics are necessary in order to further improve the quantitative accuracy of ChemLith. One important modification would be to take into account the time dependence of the optical density of the exposed region during radiation damage, especially at the characteristic energies. At present (eq 2) the sample OD is considered to be fixed during the exposure when the radiation dose is lower than or comparable to the critical dose, but in fact it does change since the spectrum changes due to the radiation damage. A further factor that needs to be included is mass loss, which is a significant factor for PMMA, PPC, and PEC. Both the damage to the functional groups and the mass loss follow the same first-order damage kinetics as are assumed in this work.[2,7−11,19] The strategies described here for chemically selective patterning of trilayer polymer systems are considered generally applicable for the development of polymer systems with even more layers, though finding suitable candidate polymers may be a challenge, as much for chemical compatibility reasons as for the specifics of X-ray absorption spectra and critical dose properties.

In order to make reproducible patterning, a number of factors need to be considered, including film uniformity, accuracy of energy scales, microscope focus quality, higher order light, point spacing in the pattern, etc. Variation in the thin film thickness in the area the pattern is written may be one important source of differences between the experimental and the simulated results. This would introduce irregularities in the pattern, which would not be present in the simulation, since it assumes that the layer thicknesses are uniform. If one included a film thickness map to the input of ChemLith, the simulations could be further improved. The accuracy of the photon energy influences the patterning selectivity since the best results are obtained when the energy corresponds to the maximum of the characteristic NEXAFS peaks. Energy scale errors as small as 0.1 eV will influence the patterning results. The focus quality is also important, not just to the sharpness of the patterns but, even more critically, to the rate of pattern generation. When the pattern is generated with the beam out of focus, blurred patterns (e.g., Figure 4f−i) or even no pattern can result. Below 120 nm, the point spacing in the pattern generation has relatively little influence on the patterning results. For example, the pattern of Figure 5a was generated twice, first using a point spacing of 67 nm and second using a point spacing of 101 nm. The outcomes were very similar (results not shown), which is a direct consequence of the damage spreading effect.

In summary, multilayer polymer structures combined with selected energy irradiation provide chemically selective patterning of polymers and direct-write patterning at the submicron scale. This work complements other efforts in soft X-ray lithography such as soft X-ray patterning of polymer thin films[8,20] and self-assembled monolayers (SAMs).[21−23] The latter examples involved simple patterns such as square pads, and there was no manipulation of the photon energy or exposure protocol to control and optimize the radiation damage. Patterning with tuned soft X-rays, as in this work, exploits differential spectrochemical sensitivity and thereby provides "added value" relative to single energy or broad band X-ray lithography. In addition to the direct-write capability and good spatial resolution, potential applications of this approach may be found in advanced device fabrication and development, which usually involve multilayer and multicomponent structures, or require multilayer resists[24,25] in the lithography stage. Other applications of this technique may be found in radiation modification of materials such as SAMs and nanoparticles for specific purposes such as tailored modification of functional groups and physicochemical properties, e.g., hydrophilic/hydrophobic patterning of a surface, and other types of nanofabrication involving radiation-induced reactions. The principles and examples presented in this work are expected to stimulate further research and possibly lead to practical applications of this novel technique.

Acknowledgment. This research is supported by NSERC (Canada), the Canadian Foundation for Innovation (CFI), and the Canada Research Chair Program. We thank Tolek Tyliszczak for writing the pattern generation component of STXM_control with which these patterns were written. We thank David Kilcoyne for expert maintenance of STXM5.3.2 and Daniel Hernandez-Cruz for assistance with operating the STXM. Construction and operation of the STXM5.3.2 microscope is supported by NSF DMR-9975694, DOE DE-FG02-98ER45737, Dow Chemical, NSERC, and CFI. The Advanced Light Source is supported by the Director, Office of Energy Research, Office of Basic Energy Sciences, Materials Sciences Division of the U.S. Department of Energy, under Contract No. DE-AC03-76SF00098.

References and Notes

(1) Stöhr, J. *NEXAFS Spectroscopy*; Springer Tracts in Surface Science 25; Springer: Berlin, 1992.

(2) Wang, J.; Stöver, H. D. H.; Hitchcock, A. P.; Tyliszczak, T. *J. Synchrotron Radiat.* **2007**, *14*, 181.

(3) Ade, H. In *Experimental Methods in the Physical Sciences*; Samson, J. A. R., Ederer, D. L., Eds.; Academic Press: New York, 1998; Vol. 32, p 225.

(4) Ade, H.; Urquhart, S. G. In *Chemical Applications of Synchrotron Radiation*; Sham, T. K., Ed.; World Scientific Publishing: River Edge, NJ, 2002.

(5) Warwick, T.; Ade, H.; Kilcoyne, D.; Kritscher, M.; Tyliszczak, T.; Fakra, S.; Hitchcock, A.; Hitchcock, P.; Padmore, H. *J. Synchrotron Radiat.* **2002**, *9*, 254.

(6) Kilcoyne, A. L. D.; Tyliszczak, T.; Steele, F.; Fakra, S.; Hitchcock, P.; Franck, K.; Anderson, E.; Harteneck, B.; Rightor, E. G.; Mitchell, G. E.; Hitchcock, A. P.; Yang, L.; Warwick, T.; Ade, H. *J. Synchrotron Radiat.* **2003**, *10*, 125.

(7) Wang, J.; Morin, C.; Li, L.; Hitchcock, A. P.; Scholl, A.; Doran, A. *J. Electron Spectrosc. Relat. Phenom.* **2007**, in press.

(8) Zhang, X.; Jacobsen, C.; Lindaas, S.; Williams, S. *J. Vac. Sci. Technol., B* **1995**, *13*, 1477.

(9) Rightor, E. G.; Hitchcock, A. P.; Ade, H.; Leapman, R. D.; Urquhart, S. G.; Smith, A. P.; Mitchell, G.; Fischer, D.; Shin, H. J.; Warwick, T. *J. Phys. Chem. B* **1997**, *101*, 1950.

(10) Beetz, T.; Jacobsen, C. *J. Synchrotron Radiat.* **2002**, *10*, 280.

(11) Coffey, T.; Urquhart, S. G.; Ade, H. *J. Electron Spectrosc. Relat. Phenom.* **2002**, *122*, 65.

(12) aXis2000 is an application written in Interactive Data Language. It is available free for noncommercial applications at http://unicorn.mcmaster.ca/aXis2000.html.

(13) Egerton, R. F.; Li, P.; Malac, M. *Micron* **2004**, *35*, 399.

(14) Frey, S.; Rong, H.-T.; Heister, K.; Yang, Y.-J.; Buck, M.; Zharnikov, M. *Langmuir* **2002**, *18*, 3142.

(15) Attwood, D. *Soft X-rays and Extreme Ultraviolet Radiation, Principles and Applications*; Cambridge University Press: Cambridge, U.K., 2000.

(16) Rabek, J. F. *Photostabilization of Polymers: Principles and Applications*; Elsevier: Oxford, England, 1990.

(17) Ito, H.; Willson, C. G. *Polym. Eng. Sci.* **1983**, *23*, 1012.

(18) Nakano, A.; Okamoto, K.; Yamamoto, Y.; Kozawa, T.; Tagawa, S.; Kai, T.; Nemoto, H. *Jpn. J. Appl. Phys.* **2005**, *44*, 5832.

(19) Richter, A. G.; Guico, R.; Shull, K.; Wang, J. *Macromolecules* **2006**, *39*, 1545.

(20) Choi, J.; Manohara, H. M.; Morikawa, E.; Sprunger, P. T.; Dowben, P. A.; Palto, S. P. *Appl. Phys. Lett.* **2000**, *76*, 381.

(21) La, Y.-H.; Jung, Y. J.; Kim, H. J.; Kang, T.-H.; Ihm, K.; Kim, K.-J.; Kim, B.; Park, J. W. *Langmuir* **2003**, *19*, 4390.

(22) Klauser, R.; Huang, M.-L.; Wang, S.-C.; Chen, C.-H.; Chuang, T. J.; Terfort, A.; Zharnikov, M. *Langmuir* **2004**, *20*, 2050.

(23) Klauser, R.; Chen, C.-H.; Huang, M.-L.; Wang, S.-C.; Chuang, T. J.; Zharnikov, M. *J. Electron Spectrosc. Relat. Phenom.* **2005**, *144*−*147*, 393.

(24) Berreman, D. W.; Bjorkholm, J. E.; Becker, M.; Eichner, L.; Freeman, R. R.; Jewell, T. E.; Mansfield, W. M.; MacDowell, A. A.; O'Malley, M. L.; Raab, E. L.; Silfvast, W. T.; Szeto, L. H.; Tennant, D. M.; Waskiewicz, W. K.; White, D. L.; Windt, D. L.; Wood, O. R., II. *Appl. Phys. Lett.* **1990**, *56*, 2180.

(25) Rooks, M. J.; Eugster, C. C.; del Alamo, J. A.; Snider, G. L.; Hu, E. L. *J. Vac. Sci. Technol., B* **1991**, *9*, 2856.